High resolution corneal and single pulse imaging with line field spectral domain optical coherence tomography

Samuel Lawman,[1,2] Yue Dong,[1] Bryan M. Williams,[2] Vito Romano,[3] Stephen Kaye,[2,3] Simon P. Harding,[2,3] Colin Willoughby,[2,3] Yao-Chun Shen,[1,*] and Yalin Zheng[2,3]

[1]*Department of Electrical Engineering and Electronics, University of Liverpool, Liverpool, L69 3GJ, UK*
[2]*Department of Eye and Vision Science, University of Liverpool, Liverpool, L7 8TX, UK*
[3]*St. Paul's Eye Unit, Royal Liverpool University Hospital, Liverpool L7 8XP, UK*
[*]*Y.C.Shen@liverpool.ac.uk*

Abstract: We report the development of a Spectral Domain Line Field Optical Coherence Tomography (LF-OCT) system, using a broad bandwidth and spatial coherent Super-Continuum (SC) source. With conventional quasi-Continuous Wave (CW) setup we achieve axial resolutions up to 2.1 μm in air and 3D volume imaging speeds up to 213 kA-Scan/s. Furthermore, we report the use of a single SC pulse, of 2 ns duration, to temporally gate an OCT B-Scan image of 70 A-Scans. This is the equivalent of 35 GA-Scans/s. We apply the CW setup for high resolution imaging of the fine structures of a human cornea sample *ex-vivo*. The single pulse setup is applied to imaging of a coated pharmaceutical tablet. The fixed pattern noise due to spectral noise is removed by subtracting the median magnitude A-Scan. We also demonstrate that the Fourier phase can be used to remove aberration caused artefacts.

OCIS codes: (110.4500) Optical coherence tomography; (170.4500) Optical coherence tomography; (320.7100) Ultrafast measurements; (120.5050) Phase measurement.

References and links

1. A. F. Fercher, C. K. Hitzenberger, G. Kamp, and S. Y. Elzaiat, "Measurement of intraocular distances by backscattering spectral interferometry," Opt. Commun. **117**(1-2), 43–48 (1995).
2. S. R. Chinn, E. A. Swanson, and J. G. Fujimoto, "Optical coherence tomography using a frequency-tunable optical source," Opt. Lett. **22**(5), 340–342 (1997).
3. D. Huang, E. A. Swanson, C. P. Lin, J. S. Schuman, W. G. Stinson, W. Chang, M. R. Hee, T. Flotte, K. Gregory, C. A. Puliafito, and J. G. Fujimoto, "Optical coherence tomography," Science **254**(5035), 1178–1181 (1991).
4. A. F. Fercher, W. Drexler, C. K. Hitzenberger, and T. Lasser, "Optical coherence tomography - principles and applications," Rep. Prog. Phys. **66**(2), 239–303 (2003).
5. J. L. B. Ramos, Y. Li, and D. Huang, "Clinical and research applications of anterior segment optical coherence tomography - a review," Clin. Experiment. Ophthalmol. **37**(1), 81–89 (2009).
6. M. Adhi and J. S. Duker, "Optical coherence tomography--current and future applications," Curr. Opin. Ophthalmol. **24**(3), 213–221 (2013).
7. R. Leitgeb, C. Hitzenberger, and A. Fercher, "Performance of fourier domain vs. time domain optical coherence tomography," Opt. Express **11**(8), 889–894 (2003).
8. M. Choma, M. Sarunic, C. Yang, and J. Izatt, "Sensitivity advantage of swept source and Fourier domain optical coherence tomography," Opt. Express **11**(18), 2183–2189 (2003).
9. M. F. Kraus, B. Potsaid, M. A. Mayer, R. Bock, B. Baumann, J. J. Liu, J. Hornegger, and J. G. Fujimoto, "Motion correction in optical coherence tomography volumes on a per A-scan basis using orthogonal scan patterns," Biomed. Opt. Express **3**(6), 1182–1199 (2012).
10. A. F. Zuluaga and R. Richards-Kortum, "Spatially resolved spectral interferometry for determination of subsurface structure," Opt. Lett. **24**(8), 519–521 (1999).
11. T.-U. Nguyen, M. C. Pierce, L. Higgins, and T. S. Tkaczyk, "Snapshot 3D optical coherence tomography system using image mapping spectrometry," Opt. Express **21**(11), 13758–13772 (2013).
12. B. Grajciar, M. Pircher, A. Fercher, and R. Leitgeb, "Parallel Fourier domain optical coherence tomography for in vivo measurement of the human eye," Opt. Express **13**(4), 1131–1137 (2005).

#263196 Received 13 Apr 2016; revised 20 May 2016; accepted 23 May 2016; published 27 May 2016

13. Y. Zhang, J. Rha, R. Jonnal, and D. Miller, "Adaptive optics parallel spectral domain optical coherence tomography for imaging the living retina," Opt. Express **13**(12), 4792–4811 (2005).
14. Y. Nakamura, S. Makita, M. Yamanari, M. Itoh, T. Yatagai, and Y. Yasuno, "High-speed three-dimensional human retinal imaging by line-field spectral domain optical coherence tomography," Opt. Express **15**(12), 7103–7116 (2007).
15. S. Uttam and Y. Liu, "Fourier phase in Fourier-domain optical coherence tomography," J. Opt. Soc. Am. A **32**(12), 2286–2306 (2015).
16. M. H. De la Torre-Ibarra, P. D. Ruiz, and J. M. Huntley, "Double-shot depth-resolved displacement field measurement using phase-contrast spectral optical coherence tomography," Opt. Express **14**(21), 9643–9656 (2006).
17. M. J. Briones-R, M. H. De La Torre-Ibarra, F. Mendoza-Santoyo, and J. Pedroza-G, "Simultaneous birefringence imaging and depth phase resolved measurement using a Fourier domain OCT system," Opt. Lasers Eng. **68**, 104–110 (2015).
18. R. N. Graf, W. J. Brown, and A. Wax, "Parallel frequency-domain optical coherence tomography scatter-mode imaging of the hamster cheek pouch using a thermal light source," Opt. Lett. **33**(12), 1285–1287 (2008).
19. J. Zhong, S. Zhong, Q. Zhang, and L. Yao, "Two-dimensional optical coherence tomography for real-time structural dynamical characterization," Opt. Lasers Eng. **66**, 74–79 (2015).
20. R. R. Alfonso, ed., *The Super Continuum Laser Source*, 2nd ed. (Springer, 2006).
21. F. E. Robles, C. Wilson, G. Grant, and A. Wax, "Molecular imaging true-colour spectroscopic optical coherence tomography," Nat. Photonics **5**(12), 744–747 (2011).
22. E. Bordenave, E. Abraham, G. Jonusauskas, J. Oberle, and C. Rulliere, "Single-shot correlation system for longitudinal imaging in biological tissues," Opt. Commun. **208**(4-6), 275–283 (2002).
23. M. S. Muller, P. J. L. Webster, and J. M. Fraser, "Time-gated Fourier-domain optical coherence tomography," Opt. Lett. **32**(22), 3336–3338 (2007).
24. S. Moon, S. W. Lee, and Z. Chen, "Reference spectrum extraction and fixed-pattern noise removal in optical coherence tomography," Opt. Express **18**(24), 24395–24404 (2010).
25. J. P. McClure, "The Schmidt-Czerny-Turner spectrograph," Proc. SPIE **9189**, 91890C (2014).
26. Z. H. Ma, R. K. Wang, F. Zhang, and J. Q. Yao, "Spectral optical coherence tomography using two-phase shifting method," Chin. Phys. Lett. **22**(8), 1909–1912 (2005).
27. C. Li, J. A. Zeitler, Y. Dong, and Y.-C. Shen, "Non-destructive evaluation of polymer coating structures on pharmaceutical pellets using full-field optical coherence tomography," J. Pharm. Sci. **103**(1), 161–166 (2014).
28. R. Tripathi, N. Nassif, J. S. Nelson, B. H. Park, and J. F. de Boer, "Spectral shaping for non-Gaussian source spectra in optical coherence tomography," Opt. Lett. **27**(6), 406–408 (2002).
29. J. Gong, B. Liu, Y. L. Kim, Y. Liu, X. Li, and V. Backman, "Optimal spectral reshaping for resolution improvement in optical coherence tomography," Opt. Express **14**(13), 5909–5915 (2006).
30. D. Marks, P. S. Carney, and S. A. Boppart, "Adaptive spectral apodization for sidelobe reduction in optical coherence tomography images," J. Biomed. Opt. **9**(6), 1281–1287 (2004).
31. M. A. Choma, A. K. Ellerbee, C. Yang, T. L. Creazzo, and J. A. Izatt, "Spectral-domain phase microscopy," Opt. Lett. **30**(10), 1162–1164 (2005).
32. B. Grajciar, Y. Lehareinger, A. F. Fercher, and R. A. Leitgeb, "High sensitivity phase mapping with parallel Fourier domain optical coherence tomography at 512 000 A-scan/s," Opt. Express **18**(21), 21841–21850 (2010).
33. U. D. o. Defense, "MIL-STD-150A," (1959).
34. D. Williams, Y. Zheng, F. Bao, and A. Elsheikh, "Fast segmentation of anterior segment optical coherence tomography images using graph cut," Eye Vis (Lond) **2**(1), 1 (2015).
35. T. Huo, C. Wang, X. Zhang, T. Chen, W. Liao, W. Zhang, S. Ai, J. C. Hsieh, and P. Xue, "Ultrahigh-speed optical coherence tomography utilizing all-optical 40 MHz swept-source," J. Biomed. Opt. **20**(3), 030503 (2015).
36. H. Lin, R. K. May, M. J. Evans, S. Zhong, L. F. Gladden, Y. Shen, J. A. Zeitler, R. K. May, and S. Zhong, "Impact of processing conditions on inter-tablet coating thickness variations measured by Terahertz in-line sensing," J. Pharm. Sci. **104**(8), 2513–2522 (2015).
37. J. S. Titiyal, M. Kaur, R. Falera, C. P. Jose, and N. Sharma, "Evaluation of time to donor lenticule apposition using intraoperative optical coherence tomography in descemet stripping automated endothelial keratoplasty," Cornea **35**(4), 477–481 (2016).
38. D. A. Kumar, H. S. Dua, A. Agarwal, and S. Jacob, "Postoperative spectral-domain optical coherence tomography evaluation of pre-Descemet endothelial keratoplasty grafts," J. Cataract Refract. Surg. **41**(7), 1535–1536 (2015).
39. L. De Benito-Llopis, J. S. Mehta, R. I. Angunawela, M. Ang, and D. T. Tan, "Intraoperative anterior segment optical coherence tomography: a novel assessment tool during deep anterior lamellar keratoplasty," Am. J. Ophthalmol. **157**(2), 334 (2014).
40. M. A. Shousha, C. L. Karp, A. P. Canto, K. Hodson, P. Oellers, A. A. Kao, B. Bielory, J. Matthews, S. R. Dubovy, V. L. Perez, and J. Wang, "Diagnosis of ocular surface lesions using ultra-high-resolution optical coherence tomography," Ophthalmology **120**(5), 883–891 (2013).
41. L. M. Vajzovic, C. L. Karp, P. Haft, M. A. Shousha, S. R. Dubovy, V. Hurmeric, S. H. Yoo, and J. Wang, "Ultra high-resolution anterior segment optical coherence tomography in the evaluation of anterior corneal dystrophies and degenerations," Ophthalmology **118**(7), 1291–1296 (2011).

#263196 Received 13 Apr 2016; revised 20 May 2016; accepted 23 May 2016; published 27 May 2016

42. M. A. Shousha, V. L. Perez, J. Wang, T. Ide, S. Jiao, Q. Chen, V. Chang, N. Buchser, S. R. Dubovy, W. Feuer, and S. H. Yoo, "Use of ultra-high-resolution optical coherence tomography to detect in vivo characteristics of Descemet's membrane in Fuchs' dystrophy," Ophthalmology **117**(6), 1220–1227 (2010).
43. S. Wu, A. Tao, H. Jiang, Z. Xu, V. Perez, and J. Wang, "Vertical and horizontal corneal epithelial thickness profile using ultra-high resolution and long scan depth optical coherence tomography," PLoS One **9**(5), e97962 (2014).
44. V. Hurmeric, S. H. Yoo, A. Galor, A. P. Canto, and J. Wang, "Atypical presentation of Salzmann nodular degeneration diagnosed with ultra-high-resolution optical coherence tomography," Ophthalmic Surg. Lasers Imaging **42**(42), e122–e125 (2011).

1. Introduction

Scanning Point (SP) spectrometer based Spectral Domain (SD) [1] and Swept Source (SS) [2] arrangements have become the standard Optical Coherence Tomography (OCT) [3, 4] setups in ophthalmic imaging [5, 6]. The first reason for this is that Fourier Domain (FD) (including SD and SS) OCT has higher intrinsic Signal to Noise Ratio (SNR) than earlier Time Domain (TD) systems [7, 8]. The second reason is that SP configuration gives confocal gating, which removes out of focus light and improves image quality. However, motion artefacts are a profound problem for *in-vivo* imaging with SP OCT [9]. In particular, heartbeat and respiration will cause distortion of the axial positions between A-scans. This problem has been alleviated by increasing scanning speed or introducing alignment solutions, but cannot be entirely resolved.

In SP OCT, the time taken to sequentially capture A-Scans determines the image collection time (temporal gate). To increase the imaging speed and maintain the SNR, the intensity of light at the measured spot has to be increased. For *in-vivo* ophthalmic imaging, there will be a limit on how high the intensity of the spot can be before it potentially causes damage. This is a fundamental limit on the maximum theoretical imaging speeds for ophthalmic SP OCT systems.

Line Field SD-OCT (LF-OCT) [10] captures a whole cross-sectional image (B-Scan) or even a three dimensional volume [10, 11] in a single shot, instead of just a single A-Scan. It does this by using an imaging spectrograph. This parallel detection of A-Scans in a LF-OCT configuration offers several advantages over traditional SP-OCT systems. Firstly the motion-related image distortion and artefacts in a B-scan map can be significantly reduced, due to the lack of time difference between A-Scans. Secondly, since the probe beam is focused as a line at the sample surface, it can achieve a higher imaging speed (and SNR) at a lower illuminating intensity. This enables higher *in-vivo* imaging speeds with lower risk of damage. LF-OCT retains confocal gating in one lateral dimension.

Previously LF-OCT systems constructed with Super Luminescent Diode (SLD) sources have been used for *in-vivo* imaging of the cornea [12] and retina [13, 14]. Additionally, the Fourier phase [15] information from SLD LF-OCT systems has been used to map deformation of corneas with 10 nm sensitivity [16, 17]. However, the limited bandwidths of SLD based sources do not allow axial resolution much beyond 5 μm. Using thermal light sources in LF-OCT, axial resolution of nearly 1 μm has been demonstrated [18, 19]. However, the low intensity of spatially incoherent thermal light sources means that they are not suitable for *in-vivo* or high-speed imaging.

Super Continuum (SC) light sources take relative narrow bandwidth laser pulses and pass them through non-linear optical fibres, which massively increases the bandwidth [20]. The result of this process is a single spatial coherence mode output with a typical continuous spectral coverage of 400-2000 nm. Using the visible part of the SC output, a LF-OCT system for true-colour imaging with resolution of 1.2 μm has been demonstrated [21]. However, since the original demonstration of corneal imaging with SLD based LF-OCT [12], revisiting this application of LF-OCT with higher resolution SC sources has been overlooked. Hence the benefit of combined high resolution (<3 μm) and high speed (>100 kA-scans/s) of SC LF-OCT systems for Near Infra Red (NIR) imaging of the cornea has not been previously

#263196 Received 13 Apr 2016; revised 20 May 2016; accepted 23 May 2016; published 27 May 2016

presented. NIR light is preferential for ophthalmic OCT, as intense visible light is a hazard to the photosensitive retina.

As SC light source is pulsed, the duration of a single pulse can be used as the temporal gate of an OCT B-Scan image. B-Scan imaging with a single femto-second pulse of light and non-linear optic effective temporal ranging has been proposed [22]. This non-linear optic temporal ranging method has been applied to OCT A-Scans to give an additional axial gate, in order to exclude unwanted signals [23]. However, we are unaware of any previous method that has used a single laser pulse to produce an OCT B-Scan image. By using the 2ns width single pulse output of a SC source as the temporal gate, a B-Scan image can be collected orders of magnitude faster than could be done with a conventional SP OCT system. Due to the generation process, a single SC pulse has significant spectral noise, which leads to significant noise in the image. However, as the spectrum is the same in all A-Scans, the noise is "fixed pattern noise" and should be recoverable and removable from the image [24].

Without two dimensional confocal gating LF-OCT systems can suffer from aberrations such as chromatic aberrations of refractive lenses or "bow-tie" aberrations of uncorrected [25] toroidal Czerny-Turner spectrograph. We have found that these aberrations can lead to artefacts in the OCT images. Completely eliminating these aberrations in LF-OCT systems may not always be practical or economical, which is likely to be a significant reason that LF-OCT systems have not been widely used for *in-vivo* imaging applications yet. However, in this paper we show that the Fourier phase map contains information that can identify these aberration-related artefacts. Utilising this to supress the artefacts in digital post processing would improve image quality for a relatively simple system, without the cost and development time of including physical optical correction.

In this paper we propose to develop a high speed and high axial resolution LF-OCT system with a pulsed SC light source. Using the NIR part of the SC spectrum our LF-OCT system is able to provide a current axial resolution of 2.8 μm (in free space) at a volume image acquisition rate of 213 kA-scans/s, making it suitable for *in-vivo* studies. With a slower but wider detector, the axial resolution is improved to our bandwidth limit value of 2.1 μm and applied to *ex-vivo* imaging. An early iteration of our LF-OCT system was used to demonstrate a B-Scan image taken with a single SC pulse. Furthermore we will also present a Fourier phase differential mask to automatically identify and supress aberration caused artefacts.

2. Method

2.1 LF-OCT

Figure 1 shows the design of the LF-OCT system, where the major component parts are line illumination, a 4f [18] Linnik interferometer and an imaging Czerny-Turner spectrograph (Shamrock 303i, Andor, UK). Two SC light sources were used, one with a high (20 MHz) fixed pulse rate (WhiteLase Micro, Fianium, UK) that was used for the majority of the imaging and one with a variable low (1-20 KHz) pulse rate (SuperK COMPACT, NKT, Denmark) that was used for the single pulse image. A spectral band 700 nm (ISO 15004-2:2007 cut off for retina exposure) to 1000 nm (effective limit of silicon based detectors) was selected with a high pass and low pass filter. With the high fixed pulse rate source as used, after spectral filtering the maximum available power in the sample arm was 6.8 mW. This equates to an average of 3 μW for each of the 2160 simultaneously measured A-Scans with the sCMOS camera. Neutral density filters were used to control total power. The line field illumination was achieved by the conventional use of a cylindrical lens and objective lenses [12]. Various combinations of collection and objective lenses were used, which are given for each sample (section 2.2). All lenses were 25.4 mm in diameter. To achieve lower reference intensity without the complications of adding a neutral density filter into the reference arm, the flat side of a plano-convex lens was used as the reference. A 10 μm mechanical slit and a

#263196 Received 13 Apr 2016; revised 20 May 2016; accepted 23 May 2016; published 27 May 2016

300 l/mm grating were used. The spectrograph used two cameras: a sCMOS camera (2560 x 2160 pixels of 6.5 x 6.5µm, 30000 e- pixel well depth, 12 bit ADC, max frame rate 98.8 Hz, 5 ms electronic shutter) (Neo, Andor, UK) was used for the high-speed imaging whilst a BI CCD (2000 x 256 pixels of 15 x 15 µm, 150000 e- pixel well depth, 16 bit ADC, max frame rate 2 Hz, 40 ms minimum mechanical shutter opening and closing time (it was necessary to use ND filters to reduce the power because of the relatively long exposure time)) (iVac, Andor, UK) was used for the high-resolution imaging. The measured single image SNR (sensitivity) with the Neo and iVac camera was 71 (85) and 79 (93) dB respectively, while signal roll of at 1 mm depth with a 75mm achromatic objective lens was 12 and 15 dB respectively. Camera and spectrograph control, data acquisition, image processing and display were all done via a PC with a custom GUI built in MATLAB (Mathworks, US).

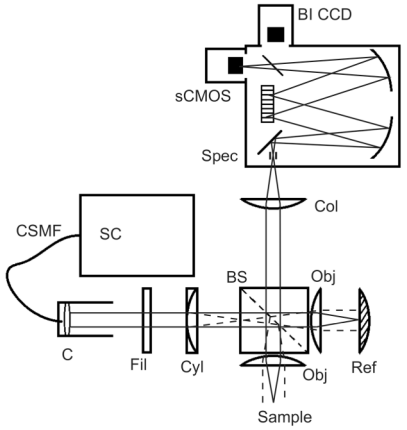

Fig. 1. The LF-OCT system. SC - Super-Continuum light source, CSMF – Continuously Single Mode Fibre. C – Collimator, Fil – Optical Filters (Bandpass and Neutral Density), Cyl – Cylindrical Lens, BS – Cube Beam Splitter. Obj – Objective Lenses, Ref – Reference Interface (Flat glass surface), Col – Collection Lens, Spec – Andor Shamrock 303i toroidal Czerny-Turner imaging spectrograph, sCMOS – Scientific Complementary Metal Oxide Semiconductor camera (Neo, Andor, UK), BI CCD – Back Illuminated Charged Couple Device camera (iVac, Andor, UK).

2.2 Samples and methods

2.2.1 Ex-vivo cornea sample

The system was used to image the layer structure of a human cornea sample. A corneo-scleral disc maintained in an organ culture medium at 31 °C was obtained from a local eye bank. It was free of corneal pathology but unsuitable for transplantation because of low donor endothelial cell density after donation (2.200 cells/mm^2). A disc of 8 mm trephine diameter was punched out from the endothelial side after transfer onto a Barron vacuum donor punch (Katena Products, New Jersey, USA). The disc was placed and attached, using fibrin glue on the epithelium side, onto a glass microscope slide. No method was used to stop drying of the sample between preparation and imaging, leading to it being partially dehydrated when imaged. It was then imaged with the LF-OCT system from the endothelial side. The reference mirror was shifted with a piezo-electric stage to give DC and common path component suppression with the method given by Ma et al [26]. 30 mm achromatic doublet objective and 100 mm achromatic doublet collection lenses were used.

2.2.2 Pharmaceutical tablet for single pulse image

To capture an image with a single pulse of SC light, the SC light source was set to operate at 1 Hz. The exposure time of the sCMOS camera was set at 1 s to match this, the light pulse

#263196 Received 13 Apr 2016; revised 20 May 2016; accepted 23 May 2016; published 27 May 2016

being the temporal gate. The sample used was a coated pharmaceutical tablet [27]. 40 mm achromatic doublet objective and collection lenses were used.

2.2.3 Sample and setup to induce high amounts of aberration image artefacts

The aberrations that induce artefacts on the OCT image are a result of the combined actions of the sample, interferometer optics and spectrograph optics on the light. The interaction of all three parts determines how far from the correct position light arrives on the detector. To induce maximum aberrations the worst choice of sample, picked from experience, and interferometer optics, non aberration-corrected lenses, were chosen. For the sample, cling film was suspended between two optical posts facing end to end but with a ~1 cm gap between them. The cling film was wrapped once over this gap and pulled tight giving a smooth, curved and freestanding layer. During the development of the system we found curved semi-specular reflecting interfaces, such as this, to be particularly susceptible to image artefacts. 100 mm plano-convex singlet objective and collection lenses were used as these introduce significantly more aberrations than the equivalent achromatic doublets.

2.3 Data processing

The measured raw spectrums are first resampled to achieve uniform spacing in angular frequency domain. To control the axial point spread function shape, a spectral window is applied to the spectrums [28–30]. This window is calculated by

$$K(\omega) = \frac{D(\omega)}{S(\omega)}, \tag{1}$$

where D(ω) is the desired spectral shape and S(ω) is the measured effective raw spectrum shape. Discrete Fourier Transform (DFT) of the spectra then gives the complex A-Scans. The complex A-Scan signal for a single scattering or reflecting point *(j)* is given by

$$I'(t) = 2.T.R.DFT\left(K(\omega).S(\omega)\right) \otimes h_j \delta_{t,\Delta t}\left(a_j + b_j i\right), \tag{2}$$

$$\text{where } \sqrt{a_j^{\,2} + b_j^{\,2}} = 1 \tag{3}$$

Here, T is the interferometer transmission constant, R is the reference surface field reflection coefficient, $\otimes$ is the convolution operator, $\delta_{t,\Delta t}$ is the Kronecker delta function, h_j is the effective field reflection coefficient of scatter j, and Δt_j is the time of flight difference between the light reflected from scatterer j and the reference interface to the detector. Time *(t)* units are converted to optical distance by $z = \frac{t.c}{2}$, where c is the speed of light. The magnitude values of Eq. (2) give the OCT images, while the complex phase angle is the pixel resolved Fourier phase [15, 31]. The method of using Fourier phase information to clean images was derived empirically from the measured Fourier phase images.

3. Results and discussion

3.1 Axial resolution, lateral resolution and demonstration of high-speed volume imaging

To quantify the axial resolution of the LF-OCT system, a flat glass surface was measured. Figure 2 inset shows one of the raw spectrums measured with the BI CCD camera and 300 l/mm grating. The main part of Fig. 2 then shows the resultant theoretical raw (line), measured raw (circles) and measured digital spectral shaped (crosses) axial Point Spread Functions (PSFs). The theoretical and measured raw PSF closely match, the LF-OCT systems Linnik based design is free from significant broadening due to dispersion. The Full Width Half Maximum (FWHM) resolution is 2.1 μm in air. Digitally shaping the spectrum to a Hann shape broadens the PSF slightly (2.4 μm FWHM in air) but achieves significant reduction of

#263196 Received 13 Apr 2016; revised 20 May 2016; accepted 23 May 2016; published 27 May 2016

side lobes. With the smaller width sCMOS camera, without changing the 300 l/mm grating, the raw resolution is reduced to 2.8 μm in air. These values are 6 times better than when LF-OCT was last demonstrated (17 μm) [12] for corneal imaging.

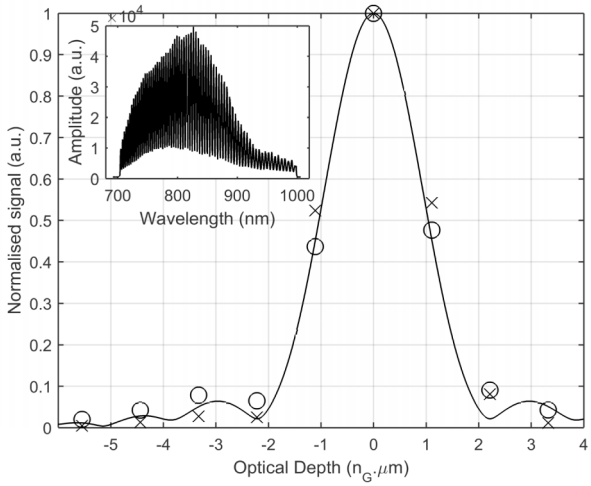

Fig. 2. Plot of the theoretical raw (padded FFT of S(ω)) (line), measured example raw (circles) and measured example digital spectral shaped (crosses) axial PSFs of the LF-OCT using the wide BI CCD camera and 300 l/mm grating. (Inset) An example raw OCT spectrum in wavelength space.

In order to quantify the lateral resolution and to demonstrate undistorted imaging at a high volume acquisition rate, a USAF 1951 target (ThorLabs, US) was used. This was mounted on a mechanical stage (ThorLabs, US) to enable 3D imaging. 30 mm achromatic doublet objective and 100 mm achromatic doublet collection lenses were used in the LF-OCT. Figure 3 is an en-face image of a USAF 1951 resolution target, from an OCT volume taken at 213 kAScans/s. This volume A-Scan rate is ~40% of the highest known value for LF-OCT reported to date [32]. However, the current system has 2.5 times the pixels per A-Scan (1280 vs 512) so per pixel is 4% faster. With 30 mm achromatic doublet objective and 100mm achromatic doublet collection lenses, the highest lateral resolution measured was 5.5 x 9 μm (per line pair resolved [33]).

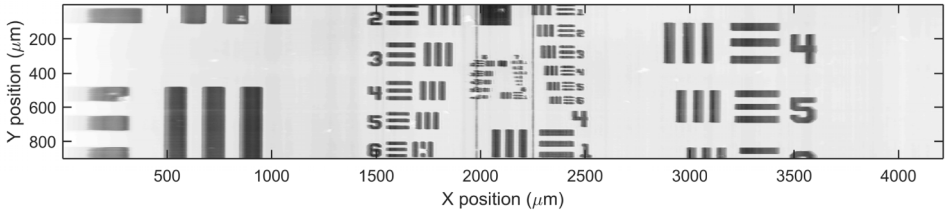

Fig. 3. En-face OCT image of USAF 1951 chart from volume taken at 213kAScans/s.

3.2 Ex-vivo corneal imaging

In order to demonstrate high resolution imaging with our LF-OCT, we measured a partially dried human cornea sample *ex-vivo*. Figure 4 shows a B-Scan image of this sample. All five of the commonly accepted layers (Endothelium, Descemet's Membrane, Stroma, Bowman's Membrane and Epithelium) are resolved. Figures 4 and 5 show the successful segmentation (red line) of the acquired image using a supervised graph search method based on [34] incorporating the energy of the Laplacian. The segmentation method for the endothelium

#263196 Received 13 Apr 2016; revised 20 May 2016; accepted 23 May 2016; published 27 May 2016

surface was modified to account for the fact that the peak signal of the strong surface reflection will correspond better to interface in this case. This allows for layers to be distinguished and measured. For presentation, the result was cleaned using a one-dimensional averaging filter. The increased axial resolution is a significant improvement on previous imaging of human corneas with LF-OCT [12], where these layers were not resolved. Table 1 gives the optical thicknesses measured from this sample, though due to the *ex vivo* nature of the sample they are not directly comparable to *in vivo* thicknesses.

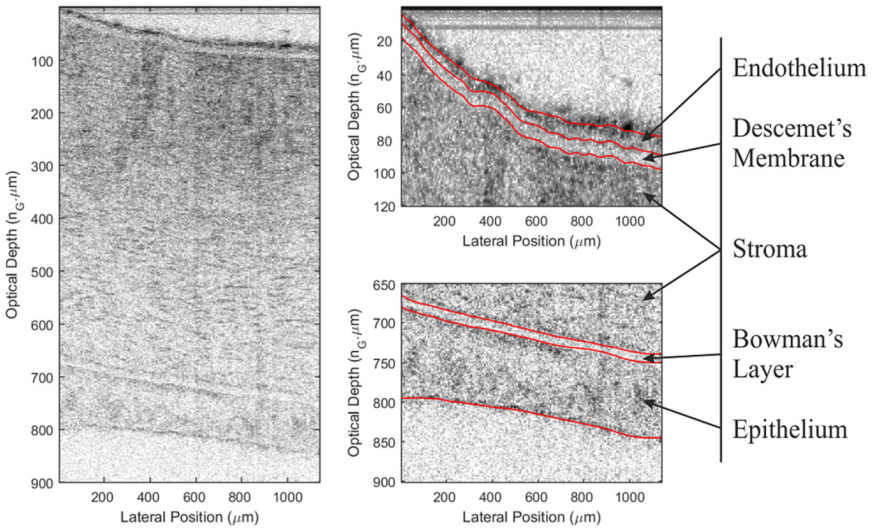

Fig. 4. (Left) Full OCT image of partially dried human cornea *ex-vivo* imaged from the back (top). (Top right) Zoom into back showing endothelium, Descemet's membrane, and stroma. (Bottom right) Zoom into front showing stroma, Bowman's membrane and Epithelium. Red lines show segmentation.

Table 1. Measured Optical Thickness of Corneal Layers*.

Layer	Mean Optical Thickness ($n_G.\mu m$)
Endothelium	8.5 (± 1.79)
Descemet's Membrane	8.9 (± <0.01)
Stroma	636.4 (± 5.16)
Bowman's Layer	9.4 (± 1.55)
Epithelium	99.5 (± 4.77)

* Optical thickness was measured using the segmentation shown above in Fig. 4.

3.3 Single pulse imaging of pharmaceutical coated tablet

In order to demonstrate LF-OCT high-speed single pulse operation, a coated pharmaceutical tablet was used as a target. Figure 5 Left shows the normalised raw OCT image taken. Boxcar averaging was used to improve the SNR. The SC spectral noise within one pulse was significant but identical in all A-Scans, which gives the significant fixed pattern noise in the image. It has previously been shown that subtracting the median complex A-Scan is an effective way of removing fixed pattern noise [24]. However, we found that subtracting the median magnitude A-Scan performed better in our case. With median complex A-Scan subtraction, fixed pattern noise 12 dB above the noise floor was still visible in the image. For magnitude A-Scan subtraction no fixed pattern artefact was visibly identifiable (<6 dB). Figure 5 Right shows a single pulse OCT image after the subtraction of median magnitude A-Scan. The image SNR is not high, with the peak signals of surface and second scattering being 23 dB and 15 dB above mean noise floor respectively. Before median magnitude subtraction these values were 10 and 4 dB respectively. The low image SNR is due to the low

#263196 Received 13 Apr 2016; revised 20 May 2016; accepted 23 May 2016; published 27 May 2016

amount of total light used for the image and un-optimised prototype design of the LF-OCT system. However, it is nevertheless sufficient to resolve the two coating layers. The surface, first clear layer and second scattering layer are all visible and the results agree well with the published data [25]. Segmenting the OCT data to identify the surfaces automatically using region based weighting with graph theory allows us to measure the optical thickness of the coating, which is 87.27 ± 3.36 n_G.µm where n_G is the refractive index of the coating. With a conventional SP OCT system, we have separately measured the range of the coating thickness to be 70 to 100 n_G.µm over the batch. To the best of our knowledge, this is the first OCT B-Scan image to be taken with a single light source pulse. The specified temporal output width of the pulse is <2 ns, which means a scanning point OCT would have to take 35 GA-Scan/s to collect the 70 A-scans used for the image in the same time. This is nearly three orders of magnitude faster than the fastest SP OCT currently known to us (40 MHz [35]). The ability to capture a whole B-scan map in a time scale of 2 ns would open up new application areas such as online monitoring of high value pharmaceutical coating process [36], where it is highly desirable to accurately measure geometrical cross sections of individual pellets that are fast tumbling in a fluid bed coater. Using the light source as the temporal gate means that this A-scan rate is independent of the camera, though the speed achieved is only applicable to a single B-scan capture. It is not applicable to a continuous stream of data where a high frame rate camera is necessary. The technique should be expandable to capture a 3D volume in a single pulse with the application of 2D to 1D mapping such as that used in [11]. Further orders of magnitude decrease of the temporal gate, thus increase of the equivalent A-Scan rate, should be possible with the use of femtosecond laser sources.

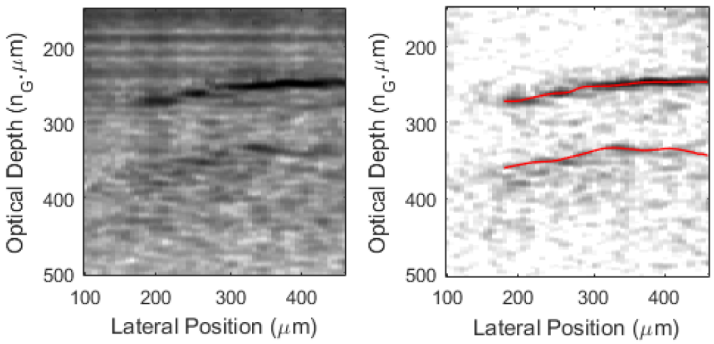

Fig. 5. (Left) Raw super-continuum single pulse LF-OCT image. (Right) Super-continuum single pulse LF-OCT image after subtraction of median magnitude A-Scan. The red lines show the segmented interfaces of the clear coating.

3.4 Fourier phase differential mask

During the development of this high-resolution LF-OCT system it was found that aberrations could cause noticeable image artefacts in front of strongly reflecting surfaces and scatters. To demonstrate this, a curved free standing cling film was imaged with a highly aberrated iteration of the LF-OCT. Figure 6(a) shows the raw B-Scan image. Significant image artefacts are visible in front of the cling film (Fig. 6 (f)), either side of the centre. Where the cling film is significantly sloped, the signal from the two interfaces is blurred (Fig. 6 (c)). Figures 6(e) and 6(h) shows the phase maps for these areas. Where the signal is from a genuine source (i.e. the position of the cling film interfaces), the phase differential between laterally adjacent pixels is low. Where the image signal was an artefact, the lateral phase gradient between adjacent pixels was quasi-random. The method is empirical and we do not have mathematical proof of why this is the case. However, it does appear that small differences in the phase are exaggerated in the artefacts to become quasi-random. This result allows the defining of a phase mask

#263196 Received 13 Apr 2016; revised 20 May 2016; accepted 23 May 2016; published 27 May 2016

$$\beta = \left| \left| \Delta_L \Psi \right| - \pi \right|, \tag{4}$$

where $\Delta_L\psi$ is the lateral pixel phase differential. The values of the mask are between 0 and π, which is then multiplied with the magnitude of the DFT to give an artefact supressed image. Figure 6(b) shows the artefact supressed image of Fig. 6(a). The quality of this image is visually significantly better. The mean signal contrast (measured against the peak interface signal) of the visibly artefacted area in front of the cling film was reduced by an average of 9 dB (as shown in Figs. 6(f) and 6(g)). A 4 dB increase was measured in the contrast between the interfaces and the non-scattering centre of the cling film (as shown in Figs. 6(c) and 6(d)). We have applied this filter to images taken with all optical setups used and found that the method improves the image quality around strong interfaces and scatterers. A small detriment to SNR is expected from the filter. The phase mask would be expected to reduce signal at interface discontinuities, though this is unlikely to be a significant issue with most samples that would undergo OCT imaging.

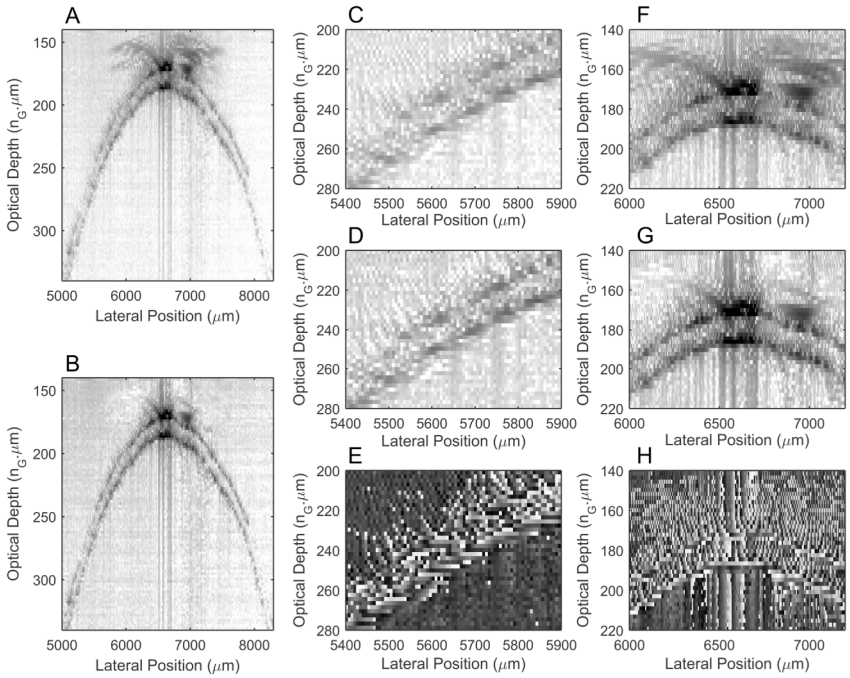

Fig. 6. (a) Aberration artefacted LF-OCT image of curved cling film. (b) The LF-OCT image after the application of the phase mask β. Zoom into side (c, d, e) and front (f, g, h) are shown before (c, f) and after (d, g) application of phase mask. The raw Fourier phase maps of these zooms are shown in (e) and (h).

6. Conclusion

A LF-OCT setup is demonstrated to be suitable for high quality ultra-high resolution imaging of the cornea and is also able to take a B-Scan image in the temporal gate of a single laser pulse.

Utilising the high bandwidth and spatial coherence of SC sources, LF-OCT is a suitable modality for the next generation of clinical OCT instruments. The high (up to 2.1 μm in air) axial resolution and volume imaging speed (up to 213 kA-Scans/s), which is desirable for future clinical OCT instruments, has been demonstrated. The system was used to image the 5 layers of a human cornea sample, which, to our knowledge, has not previously been demonstrated with LF-OCT. Anterior segment OCT has already been used to image the

#263196 Received 13 Apr 2016; revised 20 May 2016; accepted 23 May 2016; published 27 May 2016

corneal tomography, to measure corneal thickness and lamellar graft thickness [37–39]. However the application of ultra high resolution OCT to the anterior segment is potentially a new modality of imaging anterior corneal dystrophies (such as Meesmann dystrophy, Reis-Bücklers corneal dystrophy, Thiel-Behnke dystrophy, etc), posterior corneal dystrophies (such as Fuchs corneal dystrophy, posterior polymorphous corneal dystrophy, etc) [40–44]. It could characterize and localize with precision abnormalities (such as opacities, erosions, vesicles, irregularities, nodules, microcysts, guttae, thickening of layers etc) in the all layers of the cornea. In addition it could be useful in the eye banking procedure for matching donor with procedure especially for lamellar surgery such as Descemet Membrane Endothelial Keratoplasty.

Current OCT imaging speeds can be improved upon by orders of magnitude by combining LF-OCT with single pulse of a laser light source. With such a setup, the pulse width becomes the temporal gate for the whole image. This allows a B-Scan to be taken in much less time than can be achieved with current raster scanning methods. We have demonstrated an OCT B-Scan image taken with a single pulse of SC light. To the authors' knowledge, the concept of taking a B-Scan image with a single light source pulse is new to the field of OCT. The B-Scan imaging speed achieved corresponds to a SP OCT running at 35 GA-Scans/s, which is 3 orders of magnitude better than current OCT systems. To achieve this clean image from a noisy single SC pulse, the fixed pattern noise is removed by subtraction of the median magnitude A-Scan.

In addition, we also present a method to identify and remove aberration caused artefacts in LF-OCT systems without physical optical correction. The Fourier phase contains an additional layer of information to magnitude OCT images. We show that the lateral Fourier phase differential can be used to distinguish aberration caused image artefacts from the real signal. This has been applied to the automatic creation of masks to clean aberrated high-resolution LF-OCT images. The method improves the quality of certain images, particularly around strongly reflecting interfaces or scatterers.

Acknowledgments

The Ultrasensitive Optical Coherence Tomography Imaging for Eye Disease is funded by the National Institute for Health Research's i4i Programme. This paper summarises independent research funded by the National Institute for Health Research (NIHR) under its i4i Programme (Grant Reference Number II-LA-0813-20005). The views expressed are those of the authors and not necessarily those of the NHS, the NIHR or the Department of Health. This work is also partially supported by UK EPSRC (EP/L019787/1).

#263196 Received 13 Apr 2016; revised 20 May 2016; accepted 23 May 2016; published 27 May 2016